Vascular Pharmacology 156 (2024) 107397

Contents lists available at ScienceDirect

Vascular Pharmacology

journal homepage: www.elsevier.com/locate/vph

Novel NLRP3 inhibitor INF195: Low doses provide effective protection against myocardial ischemia/reperfusion injury

Simone Gastaldi [a,1], Magalì Giordano [b,1], Federica Blua [a], Chiara Rubeo [b], Valentina Boscaro [a], Saveria Femminò [b], Stefano Comità [b], Eleonora Gianquinto [a], Vanessa Landolfi [b], Elisabetta Marini [a], Margherita Gallicchio [a], Francesca Spyrakis [a], Pasquale Pagliaro [b,c,*,2], Massimo Bertinaria [a,b,*], Claudia Penna [b,c,2]

[a] Department of Drug Science and Technology, University of Turin, Via P. Giuria 9, 10125 Torino, Italy
[b] Department of Clinical and Biological Sciences, University of Turin, Regione Gonzole 10, Orbassano, 10043 Torino, Italy
[c] INRC, Bologna, Italy

ARTICLE INFO

Keywords:
NLRP3 inflammasome
Cardioprotection
Interleukin-1β

ABSTRACT

Background: Several factors contribute to ischemia/reperfusion injury (IRI), including activation of the NLRP3 inflammasome and its byproducts, such as interleukin-1β (IL-1β) and caspase-1. However, NLRP3 may paradoxically exhibit cardioprotective properties. This study aimed to assess the protective effects of the novel NLRP3 inhibitor, INF195, both *in vitro* and *ex vivo*.

Methods: To investigate the relationship between NLRP3 and myocardial IRI, we synthetized a series of novel NLRP3 inhibitors, and investigated their putative binding mode *via* docking studies. Through *in vitro* studies we identified INF195 as optimal for NLRP3 inhibition. We measured infarct-size in isolated mouse hearts subjected to 30-min global ischemia/one-hour reperfusion in the presence of three different doses of INF195 (5, 10, or 20-μM). We analyzed caspase-1 and IL-1β concentration in cardiac tissue homogenates by ELISA. Statistical significance was determined using one-way ANOVA followed by Tukey's test.

Results and conclusion: INF195 reduces NLRP3-induced pyroptosis in human macrophages. Heart pre-treatment with 5 and 10-μM INF195 significantly reduces both infarct size and IL-1β levels. Data suggest that intracardiac NLRP3 activation contributes to IRI and that low doses of INF195 exert cardioprotective effects by reducing infarct size. However, at 20-μM, INF195 efficacy declines, leading to a lack of cardioprotection. Research is required to determine if high doses of INF195 have off-target effects or dual roles, potentially eliminating both harmful and cardioprotective functions of NLRP3. Our findings highlight the potential of a new chemical scaffold, amenable to further optimization, to provide NLRP3 inhibition and cardioprotection in the ischemia/reperfusion setting.

1. Introduction

Acute myocardial infarction (AMI) stands as the primary cause of disability and mortality in the Western world [1,2]. Primary percutaneous coronary intervention (PCI) is widely acknowledged as the preferred strategy for preserving cardiac function, thereby reducing the occurrence of post-ischemic heart failure (HF) [1,3]. However, reperfusion, paradoxically, exacerbates myocardial damage by impairing mitochondrial function, contractility, and triggering cell death [2,3]. Hence, the concept of "ischemia/reperfusion injury" (IRI) has been introduced to describe these deleterious effects [3,4]. IRI encompasses oxidative stress and inflammation, both of which contribute to the

Abbreviations: NLRP3, Nucleotide-binding oligomerization domain-like receptors with a pyrin-domain 3; IL-1β, Interleukin-1β; IRI, ischemia/reperfusion injury; IS, infarct size; DMF, dimethylformamide; TFA, trifluoroacetic acid.

* Corresponding authors at: Department of Clinical and Biological Sciences, and Department of Drug Science and Technology, University of Turin, Regione Gonzole 10, Orbassano, 10043 Torino, Italy.
E-mail addresses: pasquale.pagliaro@unito.it (P. Pagliaro), massimo.bertinaria@unito.it (M. Bertinaria).

[1] These authors share the first authorship
[2] These authors share the seniorship

https://doi.org/10.1016/j.vph.2024.107397
Received 19 February 2024; Received in revised form 21 May 2024; Accepted 16 June 2024
Available online 17 June 2024

extension of the infarcted area [2,5].

The inflammatory process involves a collection of receptors known as Pattern Recognition Receptors (PRRs), which selectively bind various factors such as pathogen-associated molecular patterns (PAMPs), released during infection, and/or damage-associated molecular patterns (DAMPs), released by stressed or damaged cells. Inflammation in IRI is referred to as "*sterile inflammation*", as it is induced by DAMPs in the absence of infectious pathogens [1,6,7]. Toll-like receptors (TLRs) act as PRRs to recognize DAMPs in sterile inflammation. Subsequently, the TLRs initiate a downstream signaling cascade which also activates cytosolic multiprotein complexes, the inflammasomes, promoting the synthesis of pro-inflammatory molecules, including cytokines and interleukins (ILs) [7,8].

In the context of IRI, the role of *Nucleotide-binding oligomerization domain-like receptors with a pyrin-domain 3* (NLRP3) is emerging among inflammasomes [7]. Indeed, NLRP3 inflammasome is expressed in cells of the cardiovascular system and is upregulated after ischemia/reperfusion (IR) [9–12]. NLRP3 is a cytosolic multiprotein complex composed by an amino-terminal pyrin domain (PYD), a central nucleotide-binding domain with ATPase activity (NACHT), and a carboxy-terminal leucine-rich repeat domain (LRR) [13]. Activation of this complex, due to the binding of adenosine triphosphate (ATP) to the NACHT domain, is associated with an Apoptosis-associated Speck-like (ASC) protein containing a caspase recruitment domain and Caspase-1. Caspase-1 performs proteolytic cleavage on Gasdermin D, pro-IL-1β, and pro-IL-18 converting them into their active forms. Pyroptosis, a form of cell death, occurs when NLRP3 activates caspases to cleave off an N-terminal fragment of Gasdermin D, creating large pores in the cell membrane [1]. Thus, in the context of IRI, the NLRP3 inflammasome appears to be a master regulator of cell survival and damage [1,6–8,14–17]. Nevertheless, NLRP3 inflammasome can be involved in cardioprotective signaling [18,19].

The first line of defense against the development of heart failure still requires therapeutic interventions that lessen IRI, and NLRP3 inflammasome inhibition has been proposed as one such therapeutic treatment [7,14]. Many NLRP3 inhibitors have been developed, considering different targets and subunits of this multiprotein complex [7,20–22].

Available IL-1β blockers have been shown to reduce risk in different cardiovascular pathologies, including AMI, heart failure, myocarditis and recurrent pericarditis in phase Ib-III clinical trials [7]. Inhibition of the NLRP3 inflammasome upstream of IL-1β production may be an even more effective strategy.

In this work, we synthesized a new series of NLRP3 inhibitors to specifically target the NACHT domain of NLRP3 and stabilize an inactive state of the protein. The ability of the synthesized compounds to inhibit cell pyroptosis and IL-1β release in human macrophages was determined, and compound **2** (INF195) was selected. Subsequently, we investigated the cardioprotective effects of INF195 using an *ex vivo* mouse heart model, wherein the inhibitor was administered prior to an IR protocol. To assess INF195's protective actions, we analyzed IL-1β and active caspase-1 levels, as well as infarct size at the end of reperfusion.

2. Materials and methods

2.1. General experimental procedures for the synthesis of new compounds

All reactions underwent monitoring *via* Thin Layer Chromatography (TLC) utilizing Merck 60 F254 (0.25 mm) plates. Visualization was achieved through UV inspection (254 nm) and/or *via* the application of $KMnO_4$ (0.5 g in 100 mL 0.1 N NaOH). Organic phases were dehydrated using Na_2SO_4 as a drying agent. Flash chromatography (FC) purifications employed silica gel from Merck with 60 mesh particles. Unless explicitly stated otherwise, all reagents were utilized as supplied without additional purification. Dichloromethane underwent drying with P_2O_5 and subsequent distillation under nitrogen prior to utilization. Dimethylformamide (DMF) was stored over 3 Å molecular sieves. Anhydrous tetrahydrofuran (THF) was freshly distilled under nitrogen from sodium/benzophenone ketyl. Proton (^1H) and carbon-13 (^{13}C) nuclear magnetic resonance (NMR) spectra were acquired using a JEOL ECZR600 spectrometer operating at 600 and 151 MHz, respectively. Coupling constants (J) are reported in Hertz (Hz), and chemical shifts (δ) are expressed in parts per million (ppm), referenced to the solvent signal as an internal standard. The following abbreviations are used to denote multiplicities: s = singlet, d = doublet, t = triplet, q = quadruplet, m = multiplet, and br = broad signal. Electrospray ionization (ESI) mass spectra were obtained using a Waters Micromass Quattro Micro instrument equipped with an ESI source. The purity of the final compounds was assessed by reverse-phase high-performance liquid chromatography (RP-HPLC) using an HP1100 chromatograph system (Agilent Technologies, Palo Alto, CA, USA). The system was equipped with a quaternary pump (G1311A), a membrane degasser (G1379A), and a diode-array detector (DAD) (G1315B), which was integrated into the HP1100 system. Data analyses were conducted utilizing an HP ChemStation system (Agilent Technologies). The analytical column employed was a LiChrospher 100 C18-e (250 × 4.6 mm, 5 μm) (Merck KGaA, 64,271 Darmstadt, Germany), eluted with CH_3CN 0.1% TFA/H_2O 0.1% TFA in a variable ratio based on compound characteristics. Compounds were dissolved in the mobile phase at approximately 0.01 mg/mL concentration and injected *via* a 20 μL loop. HPLC retention times (tR) were determined at flow rates of 1.0 mL/min, and column effluent was monitored by DAD at 226 and 254 nm, with 800 nm as the reference wavelength. Sample purity was assessed as the percentage ratio between the main peak area and possible impurities at the two wavelengths, in addition to employing DAD purity analysis of the chromatographic peak. The purity of all target compounds was >95%. Complete chemical characterization of **2** (INF195) is reported in the supplementary material (Fig. S1).

The lipophilicity of INF195 and compound **5** (ClogP), was calculated by Bio-Loom for Windows software, v. 1.5, BioByte Corporation, Claremont, CA, USA. The equation a) was used to estimate the distribution constant of **5** ($ClogD^{7.4}$) considering the calculated pKa = 4.437 (Chemdraw professional version 22.0.0.22).

a) $ClogD^{7.4} = ClogP - \log\,[1 + 10^{(pH\text{-}pKa)}]$

2.1.1. General Procedure for the Preparation of compounds 1–3

3-(2-chlorophenyl)propanoic acid (1 eq) was added to a stirred solution of CDI (1 eq) in CH_2Cl_2. The reaction was stirred at room temperature for 30 min. The appropriate piperidine derivative (1 eq) was added, and the mixture stirred for 18 h. The reaction mixture was concentrated under reduced pressure. The residue was dissolved in CH_2Cl_2 and washed with water (2 × 15 mL), brine (15 mL), dried (Na_2SO_4) and concentrated under reduced pressure.

2.1.2. Ethyl 4-(3-(2-chlorophenyl)propanoyl)piperidine-1-carboxylate (1)

The reaction was run with 3-(2-chlorophenyl)propanoic acid (1.00 g, 5.42 mmol), CDI (0.88 g, 5.42 mmol), and ethyl 4-carboxypiperidine (0.834 mL, 5.42 mmol) in CH_2Cl_2 (20 mL). The crude product was purified by silica gel chromatography (PE/EtOAc 7:3) to give **1** (1.45 g, 80.7%) as a colourless oil. Rf = 0.28 (PE/EtOAc 7:3); ^1H NMR (600 MHz, $CDCl_3$) δ: 7.31 (d, J = 7.7 Hz, 1H), 7.26 (d, J = 7.4 Hz, 1H), 7.16 (m, 2H), 4.40 (d, J = 12.5 Hz, 1H), 4.11 (q, J = 7.1 Hz, 2H), 3.76 (d, J = 12.7 Hz, 1H), 3.05 (m, 2H), 3.01 (m, 1H), 2.78 (t, J = 11.5 Hz, 1H), 2.61 (dd, J = 12.6, 7.4 Hz, 2H), 2.46 (m, 1H), 1.86 (m, 2H), 1.54 (m, 2H), 1.23 (t, J = 7.1 Hz, 3H). ^{13}C NMR (151 MHz, $CDCl_3$) δ: 174.2, 170.4, 138.8, 133.9, 131, 129.6, 127.9, 127.1, 60.7, 44.9, 41.1, 41, 33.1, 29.8, 28.4, 27.9, 14.3. MS(ESI$^+$) m/z 324 / 326 $[M + H]^+$.

*2.1.3. Ethyl 3-(3-(2-chlorophenyl)propanoyl)piperidine-1-carboxylate (**2**; INF195)*

The reaction was run with 3-(2-chlorophenyl)propanoic acid (1.00 g, 5.42 mmol), CDI (0.88 g, 5.42 mmol), and ethyl 3-carboxypiperidine (0.834 mL, 5.42 mmol) in CH_2Cl_2 (20 mL). The crude product was purified by silica gel chromatography (PE/EtOAc 7:3) to give **2** (1.25 g, 70.4%) as a colourless oil. Rf = 0.28 (PE/EtOAc 7:3); ^{1}H NMR (600 MHz, $CDCl_3$) δ: 7.32 (dd, J = 7.8 Hz, 1H), 7.28–7.25 (m, 1H), 7.16–7.14 (m, 2H), 4.65 (m, 1H), 4.12 (q, J = 7.1 Hz, 2H), 3.79–3.70 (m, 1H), 3.30 (m, 1H), 3.06 (m, 2H), 2.95 (m, 1H), 2.80 (m, 1H), 2.70–2.61 (m, 2H), 2.38–225 (m, 1H), 2.05–1.97 (m, 1H), 1.74–1.69 (m, 2H), 1.43–130 (m, 1H), 1.25–1.23 (t, 3H). ^{13}C NMR (151 MHz, $CDCl_3$) δ: 173.3–172.9, 170.7–170.6, 138.9–138.8, 134–133.9, 131, 129.6, 127.9, 127.1–127.0, 60.9–60.7, 47.4–46, 43.7–42.1, 41.8–41.3, 33.2–33.1, 29.8, 27.4–27.3, 25.1–24, 14.3. The presence of splitted signals is due to the existence of rotamers. MS(ESI$^+$) *m/z* 324 / 326 $[M + H]^+$.

*2.1.4. 3-(3-(2-chlorophenyl)propanoyl)piperidine-1-carboxamide (**3**)*

The reaction was run with 3-(2-chlorophenyl)propanoic acid (1.00 g, 5.42 mmol), CDI (0.88 g, 5.42 mmol), and 3-piperidincarboxamide (0.834 mL, 5.42 mmol) in CH_2Cl_2 (20 mL). The crude product was purified by silica gel chromatography (PE/EtOAc 7:3) to give **3** (0.89 g, 45.7%) as a cream colored solid. Rf = 0.28 (PE/EtOAc 7:3); ^{1}H NMR (600 MHz, DMSO-D_6) δ: 7.40–7.35 (m, 3H), 7.27–7.23 (m, 2H), 6.84 (d, J = 25.8 Hz, 1H), 4.39–4.15 (two d, J = 12.6 Hz, 1H), 3.78 (d, J = 6.9 Hz, 1H), 3.08–2.91 (m, 1H), 2.90–2.88 (m, 2H), 2.63–2.50 (m, 2H), 2.22–2.12 (m, 1H), 1.83–1.63 (m, 1H), 1.60–1.58 (m, 2H), 1.28–1.24 (m, 1H). ^{13}C NMR (151 MHz, DMSO-D_6) δ: 175.3–175, 169.9–169.8, 139.2–139.1, 133.5–133.4, 131.3–131.2, 129.7, 128.48–128.44, 127.79–127.77, 48–45.8, 44.2–42.6, 42.4–41.9, 32.74–32.67, 29.2–29.1, 28.1–27.9, 25.4–24.5. The presence of splitted signals is due to the existence of rotamers. MS(ESI$^+$) *m/z* 295 / 297 $[M + H]^+$.

*2.1.5. 4-(3-(2-chlorophenyl)propanoyl)piperidine-1-carboxylic acid (**4**)*

Compound **1** (1.28 g, 3.93 mmol) was dissolved in a stirred solution of aqueous NaOH 2.5 N (4 mL) in ethanol (15 mL). After 12 h, the mixture was acidified with HCl 1 N (10 mL) and the ethanol was evaporated under reduced pressure. The acidic aqueous phase was extracted with CH_2Cl_2 (4 × 15 mL). The combined organic phases were washed with brine (10 mL), dried (Na_2SO_4) and concentrated under reduced pressure. The crude product was purified by silica gel chromatography (DCM/MeOH 95:5) to give **4** (1.16 g, 99.4%) as a white solid. ^{1}H NMR (600 MHz, DMSO-D_6) δ: 12.2 (s, 1H), 7.40–7.36 (m, 2H), 7.26–7.22 (m, 2H), 4.21 (d, J = 12.6 Hz, 1H), 3.77 (d, J = 12.6 Hz, 1H), 3.03–2.98 (m, 1H), 2.86 (m, 2H), 2.69–2.65 (m, 1H), 2.60–2.51 (m, 2H), 2.45–2.40 (m, 1H), 1.78 (d, J = 13.2 Hz, 2H), 1.41–1.33 (m, 2H). ^{13}C NMR (151 MHz, DMSO-D_6) δ: 176.1, 169.8, 139.2, 133.4, 131.3, 129.7, 128.5, 127.8, 44.7, 41, 40.6, 32.7, 29.2, 28.8, 28.2. MS(ESI$^-$) *m/z:* 294 / 296 $[M-H]^-$.

*2.1.6. 3-(3-(2-chlorophenyl)propanoyl)piperidine-1-carboxylic acid (**5**)*

Compound **2** (0.298 g, 0.921 mmol) was dissolved in a stirred solution of aqueous NaOH 2.5 N (1 mL) in MeOH (5 mL). After 12 h, the mixture was acidified with HCl 1 N (10 mL), and the methanol was evaporated under reduced pressure. The acidic aqueous phase was extracted with CH_2Cl_2 (4 × 15 mL). The combined organic phases were washed with brine (10 mL), dried (Na_2SO_4) and concentrated under reduced pressure. The crude product was purified by silica gel chromatography (DCM/MeOH 95:5) to give **5** (0.194 g, 74.5%) as a white solid. ^{1}H NMR (600 MHz, DMSO-D_6) δ: 12.31 (s, br, 1H), 7.37–7.32 (m, 2H), 7.22–7.19 (m, 2H), 4.38–3.70 (m, 1H), 3.68–3.65 (m, 1H), 3.30–3.27 (m, 1H), 2.98–2.87 (m, 1H), 2.86–2.84 (m, 2H), 2.66–2.54 (m, 2H), 2.34–2.19 (m, 1H), 1.90–1.82 (m, 1H), 1.62–1.48 (m, 2H), 1.30–1.26 (m, 1H). ^{13}C NMR (151 MHz, DMSO-D_6) δ: 174.91–174.88, 170–169.9, 139.2–139.1, 133.5, 131.32–131.27, 129.7, 128.5–128.4, 127.8, 47.1–45.7, 43.7–41.8, 41.2–40.6, 33.7–32.6, 29.2, 27.3–27.2, 25.1–24.1. MS(ESI$^-$) *m/z:* 294 / 296 $[M-H]^-$.

*2.1.7. General procedure for the preparation of compounds **6**–**9***

To initiate the reaction, a stirred solution containing appropriate carboxylic acid (1 eq) in 5 mL of DMF was prepared. To this solution, DIPEA (2 eq), HOBt (0.15 eq), HBTU (1.5 eq), and the appropriate amine (1.1 eq) were added at room temperature, and the mixture was stirred overnight. Subsequently, the solvent was removed under reduced pressure, and a 10% solution of $NaHCO_3$ (20 mL) was introduced. The resulting mixture was subjected to extraction with EtOAc (3 × 20 mL). The combined organic phases were washed with brine (15 mL), dried over Na2SO4, and concentrated under reduced pressure.

*2.1.8. benzyl (1-(3-(2-chlorophenyl)propanoyl)piperidine-4-carbonyl)-L-alaninate (**6**)*

The reaction was run using benzyl *L*-alaninate (0.18 g, 1.52 mmol), DIPEA (0.70 mL, 4.14 mmol), HOBt (0.03 g, 0.21 mmol), HBTU (0.92 g, 2.07 mmol) and **4** (0.300 g, 1.38 mmol) in DMF (5 mL). The crude product was purified by silica gel chromatography (PE/EtOAc/MeOH, 7:2.5:0.5) to give **6** (0.330 g, 61.5%) as a white foam. Rf = 0.22 (PE/EtOAc/MeOH 7:2:1); ^{1}H NMR (500 MHz, DMSO-D_6) δ: 7.32–7.18 (m, 8H), 7.11 (s, 1H), 5.31–5.27 (m, 2H), 4.35 (s, 1H), 3.58–3.53 (m, 2), 3.26–3.21 (m, 2H), 2.96–2.92 (m, 2H), 2.63–2.59 (m, 2H), 2.49 (s, 1H), 1.94–1.90 (m, 2H), 1.78–1.74 (m, 2H), 1.49–1.36 (m, 2H). ^{13}C NMR (151 MHz, $CDCl_3$) δ: 175.3, 173.6, 171.5, 146.9, 136.1, 133.0, 129.2, 128.9, 128.7, 127.6, 127.3, 127.1, 127.0, 126.7, 126.5, 66.4, 52.4, 44.5, 44.1, 38.8, 32.9, 30.1, 29.6, 26.3, 17.3. MS(ESI$^+$) *m/z* 457 / 459 $[M + H]^+$.

*2.1.9. tert-butyl (1-(3-(2-chlorophenyl)propanoyl)piperidine-4-carbonyl)-L-phenylalaninate (**7**)*

The reaction was run using *L*-phenylalanine *tert*-butyl ester (0.287 g, 1.52 mmol), DIPEA (0.70 mL, 4.14 mmol), HOBt (0.028 g, 0.21 mmol), HBTU (0.915 g, 2.07 mmol) and **4** (0.300 g, 1.38 mmol) in DMF (5 mL). The crude product was purified by silica gel chromatography (PE/EtOAc/MeOH, 7:2.5:0.5) to give **7** (0.330 g, 75.5%) as a white foam. Rf = 0.22 (PE/EtOAc/MeOH 7:2:1); ^{1}H NMR (600 MHz, $CDCl_3$) δ: 9.16 (d, J = 147.0 Hz, 1H), 7.35–7.27 (m, 1H), 7.27–7.05 (m, 10H), 6.13 (d, J = 38.4 Hz, 1H), 4.90–4.76 (m, 1H), 4.56–4.41 (m, 1H), 3.77 (t, J = 17.4 Hz, 1H), 3.22 (dt, J = 33.1, 16.6 Hz, 1H), 3.15–3.07 (m, 1H), 3.03 (t, J = 7.7 Hz, 2H), 2.97–2.84 (m, 1H), 2.63 (dd, J = 13.9, 5.9 Hz, 2H), 2.60 (d, J = 14.5 Hz, 1H), 2.35–2.22 (m, 1H), 1.82–1.62 (m, 2H), 1.58–1.33 (m, 2H), 1.32 (s, 9H, CH_3). MS(ESI$^+$) *m/z* 499 / 501 $[M + H]^+$.

*2.1.10. tert-butyl (1-(3-(2-chlorophenyl)propanoyl)piperidine-3-carbonyl) glycinate (**8**)*

The reaction was run using *tert*-butyl glycinate (0.910 g, 3.76 mmol), DIPEA (0.90 mL, 7.16 mmol), HOBt (0.048 g, 0.36 mmol), HBTU (2.04 g, 5.73 mmol) and **5** (0.660 g, 3.58 mmol) in DMF (5 mL). The crude product was purified by silica gel chromatography (CH_2Cl_2/MeOH, 99:1) to give **8** (0.330 g, 61.5%) as a white foam. Rf = 0.24 (PE/EtOAc/MeOH 7:2:1); ^{1}H NMR (600 MHz, $CDCl_3$) δ: 7.97 (s, 0H), 7.32–7.10 (m, 4H), 4.08 (td, J = 7.2, 2.1 Hz, 1H), 3.87–3.85 (m, 2H), 3.05–3.00 (m, 2H), 2.91 (d, J = 2.1 Hz, 2H), 2.84 (d, J = 1.0 Hz, 2H), 2.64–2.58 (m, 2H), 2.00 (t, J = 2.4 Hz, 2H), 1.40–1.44 (9H), 1.22 (qd, J = 4.8, 2.2 Hz, 2H). ^{13}C NMR (151 MHz, $CDCl_3$) δ: 172.9, 172.7, 171.2, 171.0, 170.6, 168.9, 162.6, 138.8, 138.7, 133.9, 131.1, 130.9, 129.6, 127.9, 127.1, 60.4, 46.3, 42.0, 36.6, 33.1, 28.1, 27.6, 24.6, 14.3. MS(ESI$^+$) *m/z* 409 / 411 $[M + H]^+$.

*2.1.11. benzyl (1-(3-(2-chlorophenyl)propanoyl)piperidine-3-carbonyl)-L-alaninate (**9**)*

The reaction was run using benzyl *L*-alaninate (0.242 g, 1.35 mmol), DIPEA (0.43 mL, 2.70 mmol), HOBt (0.08 g, 0.14 mmol), HBTU (0.77 g, 2.03 mmol) and **5** (0.400 g, 1.35 mmol) in DMF (5 mL). The crude product was purified by silica gel chromatography (PE/EtOAc/MeOH,

7:2.5:0.5) to give **9** (0.330 g, 61.5%) as a white foam. Rf = 0.22 (PE/EtOAc/MeOH 7:2:1); ^{1}H NMR (500 MHz, DMSO-D_6) δ: 7.32–7.18 (m, 8H), 7.11 (s, 1H), 5.31–5.27 (m, 2H), 4.35 (s, 1H), 3.58–3.53 (m, 2), 3.26–3.21 (m, 2H), 2.96–2.92 (m, 2H), 2.63–2.59 (m, 2H), 2.49 (s, 1H), 1.94–1.90 (m, 2H), 1.78–1.74 (m, 2H), 1.49–1.36 (m, 2H). ^{13}C NMR (151 MHz, $CDCl_3$) δ: 175.3, 173.6, 171.5, 146.9, 136.1, 133.0, 129.2, 128.9, 128.7, 127.6, 127.3, 127.1, 127.0, 126.7, 126.5, 66.4, 52.4, 44.5, 44.1, 38.8, 32.9, 30.1, 29.6, 26.3, 17.3. MS(ESI^+) *m/z* 457 / 459 $[M + H]^+$.

2.1.12. (1-(3-(2-chlorophenyl)propanoyl)piperidine-4-carbonyl)-L-alanine (**10**)

Compound **6** (0.26 g, 0.57 mmol) was dissolved in a suspension of Pd/C (10%, 0.061 g, 0.06 mmol) in methanol (5 mL) and stirred overnight under H_2 (1 bar). The suspension was filtered and concentrated under reduced pressure. The crude product was purified by silica gel chromatography (CH_2Cl_2 to CH_2Cl_2/MeOH 99:1) to give **10** (0.13 g, 62.1%) as a white solid. ^{1}H NMR (600 MHz, DMSO-D_6) δ: 8.24 (d, J = 7.1 Hz, 1H), 7.27–7.15 (m, 4H), 4.35 (d, J = 13.2 Hz, 1H), 4.23 (m, 1H), 3.86 (d, J = 10.1 Hz, 1H), 3.60 (s, 3H), 2.96–2.95 (m, 1H), 2.79 (t, J = 7.8 Hz, 2H), 2.40–2.37 (m, 1H), 1.68–1.64 (m, 2H), 1.43–1.33 (m, 1H), 1.25 (d, J = 7.2 Hz, 3H). ^{13}C NMR (151 MHz, DMSO-D_6) δ: 174.4, 173.8, 170.2, 142, 128.9, 128.7, 126.3, 52.3, 47.9, 44.9, 41.7, 41, 34.6, 31.3, 29.3–29.2, 28.6–28.4, 17.4. MS(ESI^-) *m/z:* 365 / 367 $[M-H]^-$.

2.1.13. (1-(3-(2-chlorophenyl)propanoyl)piperidine-4-carbonyl) phenylalanine (**11**)

Compound **7** (0.090 mg; 0.18 mmol) was dissolved in a solution of trifluoroacetic acid (2 mL) in CH_2Cl_2 (5 mL), and the mixture was stirred at room temperature overnight. The solvent was evaporated under reduced pressure. The crude product was purified by silica gel chromatography (CH_2Cl_2/MeOH 97:3) to give **11** as a white solid (0.060 mg, 74.4%). Rf = 0.51 (CH_2Cl_2 /MeOH 9:1). ^{1}H NMR (600 MHz, $CDCl_3$) δ: 9.16 (d, J = 147.0 Hz, 1H), 7.35–7.11 (m, 9H), 6.17 (s, 1H), 4.85 (t, J = 6.6 Hz, 1H), 4.50–4.47 (m, 1H), 3.78 (d, J = 13.2 Hz, 1H), 3.23 (dd, J = 13.9, 5.3 Hz, 1H), 3.10 (dd, J = 13.9, 4.6 Hz, 1H), 3.03 (t, J = 7.7 Hz, 2H), 2.97–2.84 (m, 1H), 2.65–2.58 (m, 3H), 2.28 (t, J = 11.0 Hz, 1H), 1.69 (m, 2H), 1.49–1.37 (m, 2H). ^{13}C NMR (151 MHz, $CDCl_3$) δ: 174, 173.8, 171.4, 138.3, 135.98, 135.93, 133.8, 131, 129.6, 129.5, 128.6, 128.1, 127.2, 53–52.9, 45.34–45.28, 42.6, 41.5, 37.4, 33, 29.9, 28.8–28.1, 28.5. MS(ESI^-) *m/z:* 441 / 443 $[M-H]^-$.

2.1.14. (1-(3-(2-chlorophenyl)propanoyl)piperidine-3-carbonyl)glycine (**12**)

Compound **8** (0.140 g; 0.343 mmol) was dissolved in a solution of trifluoroacetic acid (1.5 mL) in CH_2Cl_2 (15 mL), and the mixture was stirred at room temperature overnight. The solvent was evaporated under reduced pressure. The crude product was purified by silica gel chromatography (CH_2Cl_2/MeOH 97:3) to give **12** as a white solid (0.119 mg, 99.1%). Rf = 0.48 (DCM/MeOH 9:1). ^{1}H NMR (600 MHz, $CDCl_3$) δ: 7.47 (s, br, 1H), 7.32–7.30 (m, 1H), 7.22–7.12 (m, 3H), 4.61–4.60 (m, 1H), 4.15–3.98 (m, 2H), 3.72–3.70 (m, 1H), 3.45 (s, 1H), 3.02 (m, 3H), 2.83–2.53 (m, 3H), 1.90–1.86 (m, 2H), 1.72–1.70 (m, 1H), 1.29 (m, 1H). ^{13}C NMR (151 MHz, $CDCl_3$) δ: 173.2, 172.4, 171.7, 138.1, 133.9, 131.0, 129.6, 128.1, 127.2, 46.8, 45.6, 42.8, 41.7, 33.1, 29.7, 26.5, 24.9. MS(ESI^-) *m/z:* 351 / 353 $[M-H]^-$.

2.1.15. (1-(3-(2-chlorophenyl)propanoyl)piperidine-3-carbonyl)-L-alanine (**13**)

Compound **9** (0.17 g, 0.37 mmol) was dissolved in a suspension of Pd/C (10%, 0.08 g, 0.04 mmol) in methanol (5 mL) and stirred overnight under H_2 (1 bar). The suspension was filtered and concentrated under reduced pressure. The crude product was purified by silica gel chromatography (CH_2Cl_2 to CH_2Cl_2/MeOH 99:1) to give **13** (38 mg, 28.0%) as a white solid. ^{1}H NMR (600 MHz, $CDCl_3$) δ: 7.94–8.07 (m, 2H), 7.13–7.32 (m, 4H), 4.65–4.53 (m, 1H), 4.18–3.50 (m, 1H), 3.46–3.20 (m, 1H), 3.03–2.80 (m, 2H), 2.69–2.48 (m, 2H), 2.04–1.64 (m, 2H), 1.46–1.38 (m, 2H), 1.32–1.20 (m, 2H). ^{13}C NMR (151 MHz, $CDCl_3$) δ: 176.2–175.9, 173.4–172.7, 172.3–172, 140.7–140.5, 128.9–128.4 (four partially overlapping signals), 128.7, 128.5, 128.5, 126.51–126.45, 53.5, 48.5–48.3, 46.84–46.77, 45.7–44.6, 43–42.4, 35.1–35, 31.5, 27.1–26, 24.9–24.5, 18.6–17.7. MS(ESI^-) *m/z:* 365 / 367 $[M-H]^-$.

2.2. Computational studies

2.2.1. Molecular Modelling

We used as reference the X-ray crystal structure of NLRP3 NACHT domain (residues 134–676, PDB ID: 7ALV, resolution = 2.83 Å). Because of the presence of missing side chains and loops distant from the active site (residues 153–163, 178–200, 213–216, 452–462, 496–497, 513–515, 539–554, 589), Uniprot sequence of NLRP3 (Q96P20) was modelled on PDB ID structure 7ALV. Four Ramachandran outliers originating from the model (Lys194, Pro199, Lys540, Leu551) were distant from the active site in the modelled loops.

2.2.2. Molecular Docking

Maestro suite by Schrödinger, v.2022.1 was used to dock the compounds. Protein Preparation Wizard tool was employed to prepare the protein, at PROPKA pH = 7.4. Heavy atoms were minimized with restraints to RMSD 0.3 Å using the OPLS 4 force field. The ligands were prepared with the Ligprep module, generating potential states at pH = 7.4. NP3–146 ligand was self-docked in the binding site before docking each other candidate ligand using the Induced-Fit Docking (IFD) extended protocol, generating up to 80 poses. Residues Ala228, Arg351 and Arg578 were used as centroid to define the binding site, the grid was enlarged to host ligands with length up to 30 Å. For assessing the preferred binding mode, the top ten poses as determined by the IFD Score were visually examined.

2.3. In vitro NLRP3 inflammasome inhibition

2.3.1. Cell culture and treatment

Human monocytic THP-1 cells were cultured in RPMI 1640 medium (Aurogene, Rome, Italy), supplemented with fetal bovine serum (10%; Aurogene), L-glutamine (2 mM; Aurogene), penicillin (100 IU/mL; Aurogene), and streptomycin (100 mg/mL; Aurogene). The cell culture medium was refreshed every 2–3 days, and the cultures were maintained at 37 °C and 5% CO_2 in a fully humidified incubator. On the first day, THP-1 cells were seeded in 48-well plates (90,000 cells/well) and differentiated into macrophages by treatment with phorbol myristate acetate (PMA; 50 nM; 24 h; Sigma-Aldrich). After differentiation, the cells were washed twice with phosphate-buffered saline (PBS) and then primed with lipopolysaccharide (LPS; 10 μg/mL; 4 h; Sigma-Aldrich) in serum-free medium. Following priming, cells were treated with either vehicle alone or the test compound (10 μM; 1 h), and cell death was induced by ATP (5 mM, 90 min; Sigma-Aldrich). In dose-response experiments, cells were exposed to different concentrations of the compound within the range of 0.1–100 μM. At the end, supernatants were collected to quantify LDH activity and IL-1β and TNF-α release. TNF was also evaluated in supernatant collected from differentiated THP-1 pretreated with compounds (10 μM, 10 min), primed with LPS (4 h) and pulsed with ATP (5 mM, 90 min).

2.3.2. Assessment of macrophages NLRP3-dependent pyroptosis

LDH activity was measured using Cytotox 96 nonradioactive cytotoxicity assay (Promega Corporation, Madison, MI, USA) to quantify pyroptotic cell death. Absorbance was measured using the Victor X4 (PerkinElmer, Waltham, MA, USA) at λ = 490 nm. Cell death was expressed according to the manufacturer's instruction.

2.3.3. Assessment of IL-1β and TNF-α release from human macrophages

IL-1β and TNF-α release was quantified in differentiated THP-1

supernatant using Human IL-1β Uncoated ELISA kit and Human TNF-α Uncoated ELISA kit respectively (Invitrogen, Waltham, MA, USA), according to the manufacturer's instruction.

2.3.4. Assessment of cytotoxicity in THP-1 cells

THP-1 cells were seeded in 96-well culture plates at a density of 15,000 cells per well and then exposed to increasing concentrations (0.1–100 μM) of each compound. After 72 h, cell viability was assessed using the MTT assay, a colorimetric method based on the conversion of the water-soluble 3-(4,5-dimethylthiazol-2-yl)-2,5-diphenyltetrazolium bromide (MTT; Sigma-Aldrich) to an insoluble purple formazan by metabolically active cells. The concentration of formazan formed was determined by measuring absorbance at a wavelength of 570 nm using the Victor X4 (Multiskan™ FC Microplate Photometer, Thermo Scientific™).

2.4. In vitro cardiac model studies

2.4.1. Cell culture

Cardiomyoblast (H9c2) was obtained from the American Type Culture Collection (ATCC; Manassas, VA, USA). Dulbecco's Modified Eagle's Medium (DMEM) was used to grow the H9c2 samples, in addition to 10% fetal bovine serum (FBS) and 1% (*v/v*) streptomycin/penicillin (Wisent Inc., Quebec, QC, Canada), at 37 °C and 5% CO_2 [23].

2.4.2. Assessment of INF195 toxicity in cardiomyoblast

H9c2 were plated in 96-wells culture plates (3500 cells/well) and cells were serum starved for 24 h in DMEM containing 1% FBS. Subsequently, the cells were treated with increasing concentrations (0.1–50 μM) of INF195. Cell viability was measured at 24 h by the MTT assay (as above).

2.4.3. Assessment of cell permeability of INF195 and **5**

H9c2 cells were plated in 10-cm dishes (1×10^6 cells/dish) and then serum starved for 24 h in DMEM containing 1% FBS. Confluent cells were incubated for 2 h in fresh medium containing 10 μM compound **5** or INF195, washed twice in ice-cold PBS and detached with scraper. Cells were centrifuged for 5 min at 200 *g* (4 °C) and resuspended in 0.5 mL of lysis buffer (TRIS 50 mM; KCl 100 mM; $MgCl_2$ 5 mM; EDTA 1 mM). After centrifugation for 3 min at 3000 *g* (4 °C), the supernatant (cytosolic fraction) was collected. The amount of cell proteins was measured by the Brønsted-Lowry method in 50 μL of supernatant, the remaining part was stored at −80 °C until analysis. The mitochondria pellet was washed and resuspended in 320 μL of resuspension buffer (Sucrose 250 mM; K_2HPO_4 15 mM; $MgCl_2$ 2 mM; EDTA 0.5 mM); the amount of cell proteins was measured in 40 μL of supernatant, the remaining part was stored at −80 °C until analysis. Before analysis, the samples were treated with CH_3CN 1:1, filtered and then analyzed by HPLC/MS/MS.

All analyses were performed using a Shimadzu LC40 X3 UHPLC System (Shimadzu, Dusseldorf Germany), equipped with SCIEX ZenoTOF 7600 LC-MS/MS System (Sciex Pte Ltd., MA 01701 USA). UHPLC conditions: Fortis C_{18} CPS Analytical column (150 × 4.6 mm, 5 μm) was used, eluted with ACN 0.1% HCOOH/water 0.1% HCOOH, 70/30, *v/v* at a flow rate of 0.5 mL/min. The column eluate was monitored by ZenoTOF 7600 LC-MS/MS with ESI Twinsprayer Probe. The injection volume was 10 μL. MS and MS/MS data were collected for each sample. Fragmentation was performed using collision-induce dissociation (CID). Data acquisition consisted of a TOF MS scan to collect accurate mass precursor ions from 80 to 500 Da, followed by a TOF MS/MS full scan ranging from 80 to 500 Da to ensure all fragments were captured for identification. Data was acquired using SCIEX OS software 3.1. Compound **5** $[M + H]^+$ 296.1047, Rt 4.51; **INF195** $[M + H]^+$ 324.1366, Rt 7.84. Calibration curves were obtained with standard solutions of the compounds, analyzed under the same conditions as the samples; in particular, calibration curves were set up for quantification of stability experiments in a concentration range of 0.001–5 μM ($r^2 > 0.99$). The data were processed with GraphPad Prism version 7.0. The amount of compounds in the mitochondrial and cytosolic fractions was expressed as ng/mg protein.

2.5. Ex vivo cardiac model studies

Twenty-five male FVB mice (Harlan Laboratories, Udine, Italy) 10–12 weeks old and weighing 25–35 g, were maintained following the European Directive 2010/63/EU about the protection of animals being used for research reasons (n 285/2019 – PRE 669C-44).

2.5.1. Ex vivo protocol

Mice were injected with 500 U of heparin before getting anesthetized with zoletyl and xylazine (40 mg/kg and 5 mg/kg, respectively) [24]. Then, just before heart explantation, cervical dislocation was performed [25]. Hearts were quickly retrogradely perfused at 80 mmHg with Krebs-Henseleit buffer comprising NaCl (127), KCl (5.1), $NaHCO_3$ (17.7), $MgCl_2$ (1.26), $CaCl_2$ (1.5), D-glucose (11), pH 7.4 The buffer was gassed with either a 95% O_2 and 5% CO_2 mixture and the perfusion system's temperature was kept constant at 37 °C.

2.5.2. Experimental ischemia-reperfusion protocol

For all hearts, coronary perfusion pressure reached 80 mmHg and it was maintained throughout the procedure. The inhibitor, INF195, was solubilized in DMSO (Sigma, St. Louis, MO) at a concentration of 10 mM. The final concentration of DMSO (0.02%) used is not toxic in our model, as also reported in the literature [26,27]. The standard solutions were dissolved in the Krebs-Henseleit perfusion buffer to a final concentration of 5, 10, and 20 μM and used in the following groups (B, C and D; Fig. 1):

Group A, IR ($n = 8$): after stabilization (30 min), the hearts were subjected to 30 min of global, normothermic, no-flow ischemia followed by 60 min of reperfusion [28].

Group B, INF195–5 μM: At the end of 20 min of stabilization the hearts were pretreated with INF195 at a concentration of 5 μM ($n = 5$) for 10 min and then subjected to IR protocol.

Group C, INF195–10 μM: At the end of 20 min of stabilization the hearts were pretreated with INF195 at a concentration of 10 μM (n = 5) for 10 min and then subjected to IR protocol.

Group D, INF195–20 μM: At the end of 20 min of stabilization the hearts were pretreated with INF195 at a concentration of 20 μM ($n = 4$) for 10 min and then subjected to IR protocol.

Three hearts were discarded because after 20 min of stabilization they were not stable and received a higher flow than that considered normal (2–3 mL/min) for this experimental preparation [28].

2.5.3. Measurement of the Infarct Size

At the end of reperfusion, the hearts were removed from the perfusion apparatus and were dissected into two sections along a transverse line (orthogonally to a longitudinal plane). The apical portion (about one-third of the left ventricular mass) was quickly placed in liquid nitrogen and kept at −80 °C before being utilized for ELISA KIT analysis (see below), while the other half was used to measure infarct size. In particular, the left ventricles were frozen for 2 h at −20 °C at the end of each experiment. Following freezing, the hearts were sliced into 2 mm thick circumferential slices. The ventricle slices were immersed in a 0.1% nitro-blue tetrazolium solution with phosphate buffer for 20 min at 37 °C. The ImageJ processing tool was employed to determine the infarct size for every heart, slice by slice [29]. The white-colored infarcted tissue was separated from the blue area and expressed as a proportion of the total left ventricular mass, representing the risk area. Uninformed observers examined the data.

2.5.4. Determination of IL-1β and Caspase-1 in Hearts Homogenates

Heart apices, previously frozen, were lysed in a RIPA lysis buffer supplemented with protease and phosphatase inhibitors (concentration

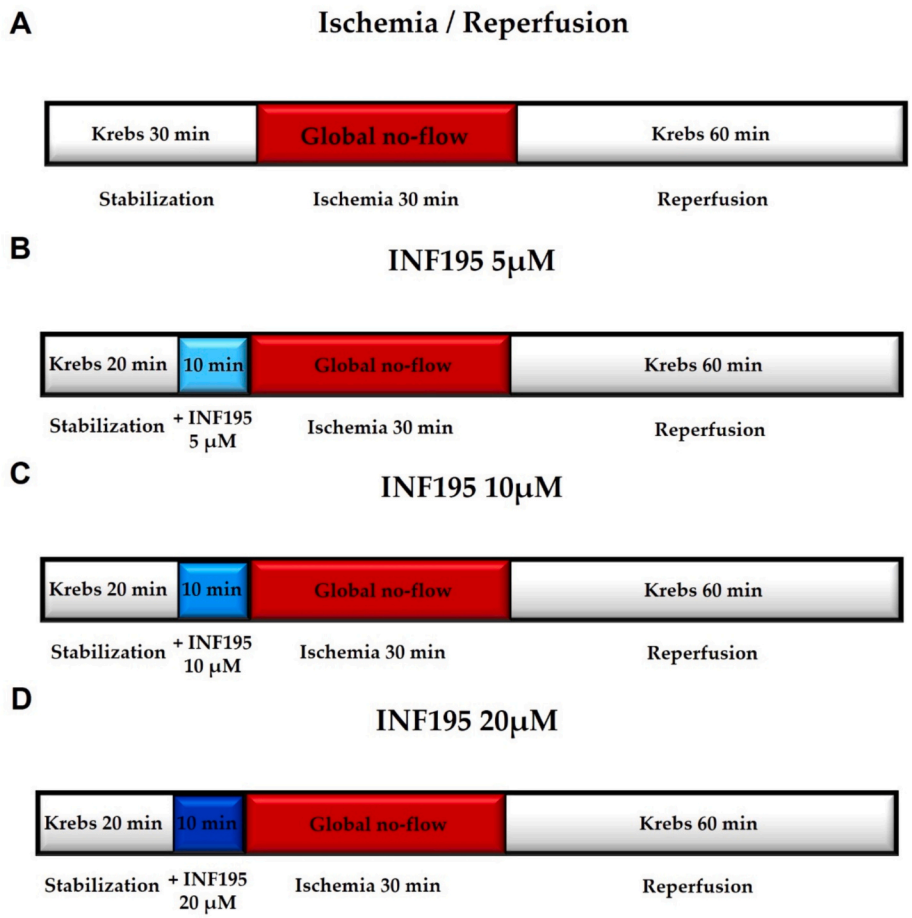

Fig. 1. The red boxes indicate the ischemic period, while the white boxes indicate the stabilization and reperfusion with the Krebs solution. **Group A** (IR): 30 min of stabilization, and 30 min of ischemia, followed by 60 min of reperfusion; **Groups B-D**: 30 min of stabilization with the infusion of INF195 at concentrations 5, 10 and 20 μM in the last 10 min; then 30 min of ischemia / 60 min of reperfusion. (For interpretation of the references to colour in this figure legend, the reader is referred to the web version of this article.)

1:1000), then we quantified the total protein with the Bradford method. Commercially available Mouse IL-1β ELISA kit (FineTest, Catalogue No EM0109-CM Wuhan, Hubei, China) and Mouse CASP1(Caspase-1) ELISA kit (FineTest, Catalogue No EM0897 Wuhan, Hubei, China) were used to measure concentrations of IL-1β and caspase-1 in tissue homogenates, according to the manufacturer's instructions [30].

2.6. Data Analysis

Dose–response curves were analyzed using a log (agonist/inhibitor) *vs* normalized response model using GraphPad Prism 9.0. EC_{50} and IC_{50} for each compound were calculated using the same program. Where indicated, the results are given as the mean ± SEM (standard error of mean). Statistical analyses were performed by one-way ANOVA using Dunnett's *post hoc* test (GraphPad).

The cardiac model studies data are presented as mean ± SEM and were analyzed using the ANOVA followed by Dunnett's and Tukey's multiple comparisons test. Statistical analyses were conducted using GraphPad Prism 8.0 software. Statistical significance was defined as a value in the $p < 0.05$ range.

3. Results and discussion

3.1. Design of novel NLRP3 inhibitors

Since 2014, our research group has been involved in the search for novel NLRP3 inhibitors. First, we explored the design of covalent NLRP3 inhibitors generating INF4E [31] and INF39 [32] that proved active, *ex vivo*, in a model of cardiovascular damage following ischemia and reperfusion [12] and *in vivo* in a model of DNBS-induced colitis [33], respectively. Later, we turned our attention to the generation of non-covalent NLRP3 inhibitors. We discovered a series of 1-(piperidin-4-yl) 1,3-dihydro-2H-benzo[*d*]imidazole-2-one derivatives [34] and of 1,3,4-oxadiazol-2-one derivatives [35] able to dampen NLRP3 activation (Fig. 2). Among the 1,3,4-oxadiazol-2-one derivatives, compound INF200 proved able to efficiently reduce cardiac and metabolic complications in an *in vivo* model of diet-induced metaflammation [35].

Taking advantage from the recently published binding site of sulfonylurea-based NLRP3 inhibitors [13,36], in this work, we applied a pharmacophore simplification approach in order to identify the minimal structural requirements capable of conferring affinity to this site in the target protein. Our working hypothesis was that the benzimidazol-2-one substructure in compound **A** (Fig. 2) could be dispensable for the binding to the target protein, while the presence of a terminal polar

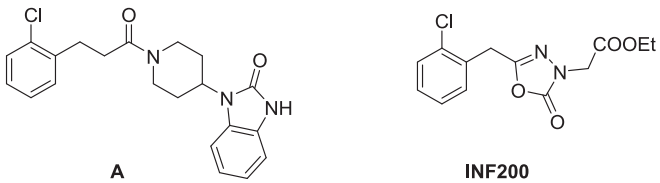

Fig. 2. Structure of compound A, a prototype benzimidazol-2-one NLRP3 inhibitor [34] and INF200, a 1,3,4-oxadiazol-2-one NLRP3 inhibitor [35].

function as in INF200 could be important to establish interactions with Arg351, a key residue in the allosteric site of the NACHT domain in NLRP3. In agreement with these considerations, molecular docking studies performed in the allosteric pocket of NLRP3 NACHT domain, evidenced that the benzimidazole-2-one moiety in compound **A** could engage Arg578 and Glu629, but not Arg351 (Fig. 3A). Thus, we envisioned that the insertion of an acidic or polar group on the piperidinyl ring in 3- or 4- position could lead to the desired interaction with Arg351, without changing the overall putative binding mode (Fig. 3B).

Based on this assumption, we designed a short series of "proof of concept" compounds lacking the benzimidazol-2-one residue to verify whether they were still able to inhibit NLRP3 activation. The structures of the proof of concept compounds synthesized in the present work are depicted in Fig. 4A. All the designed compounds bear a 3-(2-chlorophenyl)-(piperidin-1-yl)-propanamide scaffold. The piperidine ring was substituted with a carboxylic acid in position 4 (compound **4**) or in position 3 (compound **5**). This polar group can act as a hydrogen bond acceptor (HBA) in physiological conditions, while the carboxamido group, introduced in position 3 of the piperidine ring (compound **3**), can behave also as hydrogen bond donor (HBD), being not ionized at physiological pH (7.4), and less efficiently as HBA compared to the carboxylate. The ethyl ester-substituted compounds **1** and **2** (INF195) were also synthesized because of their enhanced lipophilicity and ability to cross biological membranes with respect to the corresponding acids. These esters act as the prodrug for the corresponding carboxylic acids **4** and **5** conferring some advantages in term of cell permeability as evidenced from previous work by different groups [35,37]. In derivatives **10**–**13**, the polar group was moved away from the piperidine ring by insertion of aminoacidic spacers through the formation of an amide bond in position 3 or 4 of the piperidine ring.

The insertion of the carboxylic acid (or its ester precursor) on the piperidinyl ring was designed in order to add an interaction with Arg351 in the NLRP3 NACHT domain. Induced-fit docking analysis of model compound **5** was conducted to substantiate this hypothesis. Indeed, as shown in Fig. 4B-C for compound **5**, the 2-chlorophenyl moiety retained its orientation, sandwiched between the side chain of Ile411 and Phe579, in a lipophilic sub-pocket lined by residues Ile230, Met408, Phe410, Leu411, Leu413, Tyr443, Thr524, Phe575, Phe579, Met661. Notably, the amide linker can establish hydrogen bonds with either the backbone of Ala228 or the sidechain of Arg578 while the acidic group binds to Arg351.

3.2. Synthesis of designed NLRP3 inhibitors

The designed compounds were synthesized according to the route reported in Scheme 1.

The 2-chlorophenyl propanoic acid was coupled with ethyl isonipecotate, ethyl nipecotate or piperidin-3-carboxamide, using carbonyldiimidazole (CDI) as the activating agent, to give compounds **1**–**3** in good yields. The hydrolysis of the ethyl esters in **1** and **2** (INF195) was performed using 2.5 M NaOH in EtOH at room temperature (rt) to obtain the corresponding acid derivatives **4** and **5**. The carboxylic acid **4** was coupled with benzyl *L*-alaninate or with *tert*-butyl *L*-phenylalaninate using hydroxybenzotriazole (HOBt) and *N*,*N*,*N*′,*N*′-Tetramethyl-O-(1H-benzotriazol-1-yl)uronium hexafluorophosphate (HBTU) as the activating agents and diisopropyethylamine (DIPEA) as the base to afford compounds **6** and **7**. The same protocol was used for the coupling of **5** with *tert*-butyl glycinate and benzyl *L*-alaninate to afford **8** and **9**, respectively. The obtained intermediates **6**–**9** were deprotected using classical trifluoroacetic acid-promoted deprotection (for the removal of *tert*-butyl group) or Pd-catalyzed hydrogenation (for the benzyl group) to afford the final compounds **10**–**13**.

3.3. In vitro biological characterization of the synthesized compounds and selection of compound INF195

The compounds obtained from the modulation of the piperidinamide scaffold were first evaluated at fixed concentration (10 μM) for the inhibition of NLRP3-dependent pyroptosis and IL-1β release in phorbol myristate acetate (PMA; 50 nM; 24 h)-differentiated THP-1 cells, primed with LPS (10 μg/mL; 4 h) and pulsed with ATP (5 mM; 1.5 h). Cytotoxicity was also evaluated by MTT assay in THP-1 cells treated with increasing concentration of the tested compounds (0.1–100 μM) for 72 h. The obtained results are reported in Table 1. The compounds showed a very heterogeneous efficacy, ranging from very low activity for compounds **4**, **11** and **13** to a significant inhibition of pyroptosis and IL-1b release for compounds INF195 (**2**) and **5**. Most of the compounds showed negligible toxicity in THP-1 cells with the partial exception of **10** (Table 1; Fig. S2).

Among the compounds with the polar group inserted directly on the piperidine ring (**1**–**5**) only those with the polar group in position 3 of the piperidine ring (compounds INF195, **3**, **5**) showed a significant inhibition of NLRP3-dependent pyroptotic cell death and IL-1β release (Table 1). The maximal inhibition was measured for compounds bearing the carboxylic ester (INF195) and the carboxylic acid (**5**) in this position

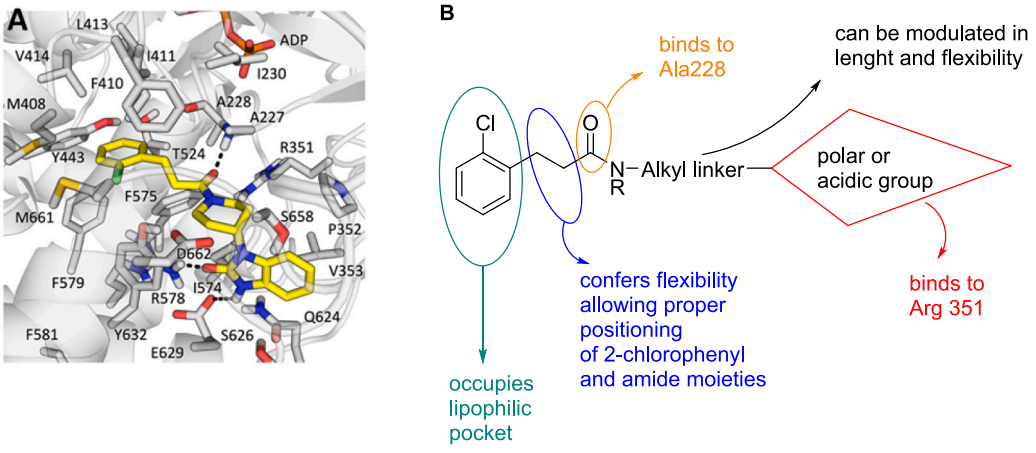

Fig. 3. Molecular docking of compound **A** (yellow). Protein is depicted as grey cartoon, residues lining the inhibitor binding site are shown as sticks and labelled with one-letter code. Inhibitors and ADP cofactors are reported as sticks, distances and angles compatible with hydrogen bonds are highlighted with black dashes. (B) General strategy used in the design of proof of concept compounds: the general structure of the designed compounds with the predicted role of each molecular portion is represented. (For interpretation of the references to colour in this figure legend, the reader is referred to the web version of this article.)

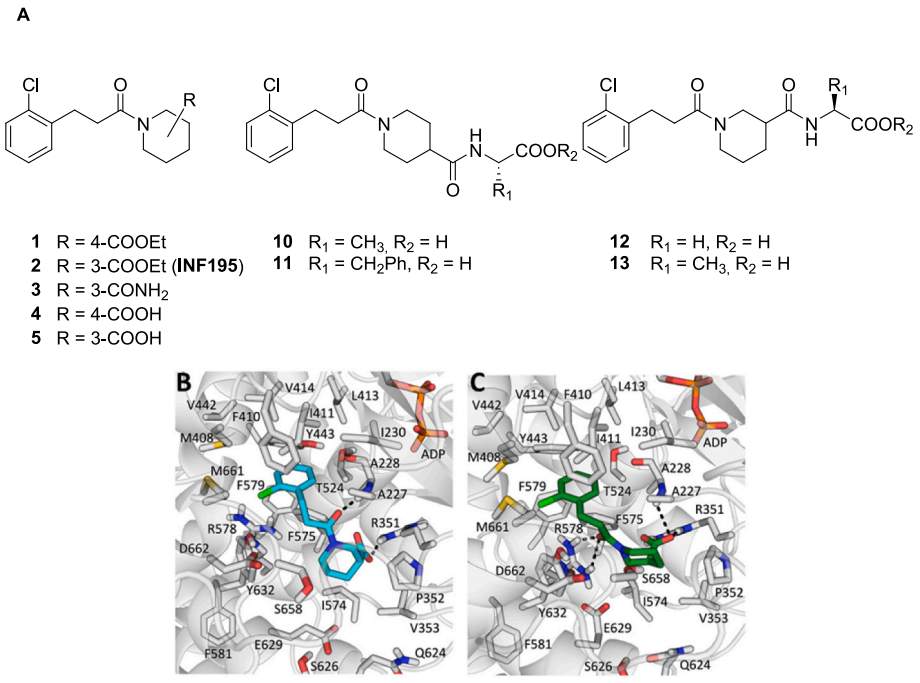

Fig. 4. (A) Detailed structures of the designed compounds **1**–**5**, **10**–**13**. Molecular docking of (B) **5** (cyan, R-stereoisomer) and (C) **5** (green, S-stereoisomer). Protein is depicted as grey cartoon, residues lining the inhibitor binding site are shown as sticks and labelled with one-letter code. Inhibitors and ADP cofactors are reported as sticks, distances and angles compatible with hydrogen bonds are highlighted with black dashes. (For interpretation of the references to colour in this figure legend, the reader is referred to the web version of this article.)

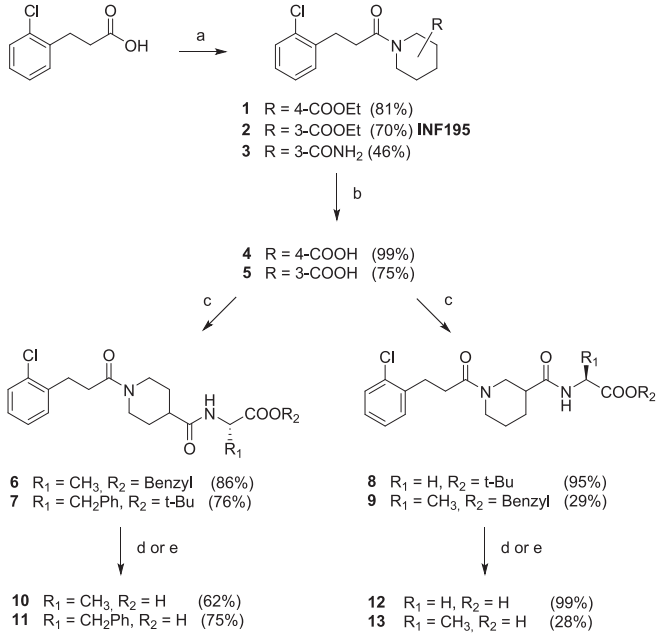

Scheme 1. Reagents and conditions: (a) (i) CDI (1 eq), CH_2Cl_2, rt., 30 min; (ii) substituted piperidine (1 eq), rt., 18 h. (b) NaOH 2.5 M (2.5 eq), EtOH, rt., 18 h. (c) aminoacid (1.1 eq), HBTU (1.5 eq), HOBt (0.1 eq), DIPEA (3 eq), DMF, 18 h. (d) TFA (10 eq), CH_2Cl_2, rt., 18 h. (e) Pd/C 10% (0.1 eq), H_2, MeOH, rt., 18 h.

with inhibition in the 30–40% range for both pyroptosis and IL-1β release. The piperidine-3-carboxyamide (compound **3**), devoid of acidic properties, revealed a reduced activity profile, compared to the corresponding ester or acid at the tested concentration of 10 μM (pyroptosis reduction: 22.7 ± 10.3%; IL-1β inhibition: 13.24 ± 1.14%). When an aminoacidic spacer was inserted between the piperidine ring and the polar residue the activity dropped dramatically, regardless of the position of the spacer on the piperidine ring. The only partial exception was represented by compound **12**, bearing a glycine residue, which was still able to exert little antipyroptotic and anti-IL-1β effects. From the first phenotypic screening, compound **5** and its ethyl ester prodrug INF195, able to generate **5** in physiological conditions (Fig. S3), emerged as the most interesting NLRP3 inhibitors of the series.

Table 1
Inhibitory effect of synthesized compounds on pyroptotic cell death and IL-1β release in differentiated THP-1 cells and cytotoxicity in THP-1 cells. [a] Pyroptosis of differentiated THP-1 cells was triggered using LPS/ATP. Data are reported as the % inhibition of pyroptosis of cells treated with 10 μM conc of test compounds *vs* vehicle-treated cells. Data are the mean ± SEM of three to five experiments run in triplicate. [b] IL-1β inhibition was measured in the cell supernatants form the same experiments. Data are reported as % inhibition ± SEM of three to five experiments run in triplicate. [c] Cytotoxicity was determined after 72 h treatment of THP-1 cells with increasing conc (0.1–100 μM) of test compounds. Data are reported as TC_{50} ± SEM of three experiments. [d] $p < 0.05$ *vs* vehicle-treated cells; [e] $p < 0.01$ *vs* vehicle-treated cells; NT = not tested.

Compound	Pyroptosis decrease[a]	IL-1β inhibition[b]	Cytotoxicity[c]
	% inhibition at 10 μM	*% inhibition at 10* μM	*TC_{50}(μM)*
1	11.0 ± 9.0	NT	> 100
2 (INF195)	32.9 ± 3.4[d]	38.0 ± 7.5[d]	> 100
3	22.7 ± 10.3	13.2 ± 1.1	> 100
4	< 10	NT	> 100
5	40.4 ± 11.9[e]	40.5 ± 5.5[d]	> 100
10	11.4 ± 6.2	< 10	74.3 ± 1.5
11	< 10	NT	> 100
12	22.8 ± 7.09	24.4 ± 8.2	> 100
13	< 10	NT	> 100

3.4. *INF195 and its predicted metabolite **5** inhibit NLRP3-driven pyroptosis and IL-1 β release in a concentration-dependent manner*

Compounds INF195 and **5** were then tested to verify the dose-

dependency of the effect and to determine an EC_{50} value for pyroptosis inhibition and IL-1β release (Fig. 5). The maximum inhibition of pyroptosis induced by compound **5** was about 70%, with an EC_{50} of 7.47 ± 3.97 μM. Compound INF195 inhibited pyroptosis only by about 40%, with an EC_{50} of 0.15 ± 0.14 μM. Both compounds inhibited IL-1β release in a dose-dependent manner. The EC_{50} were 3.63 ± 1.37 μM for INF195 and 6.45 ± 3.94 μM for **5**.

3.5. Compounds INF195 and 5 do not inhibit TNF-α release from human macrophages

To verify the absence of an effect on NF-κB signaling, the amount of TNF-α released from differentiated THP-1 triggered with LPS/ATP was measured. Both compounds INF195 and **5**, tested at 10 μM, were not able to significantly modify TNF-α release, either if incubated before or after LPS stimulation (Fig. 6).

3.6. INF195 permeates H9c2 cardiomyoblasts where it is hydrolyzed to active metabolite 5

In order to select one compound for *ex vivo* studies, we verified the ability of INF195 and **5** to penetrate inside cardiac cells by incubating both compounds (10 μM) with H9c2 cells. After 2 h, the cells were treated with lysis buffer to isolate cytosolic and mitochondrial fractions. The fractions were then analyzed using UHPLC/MS/MS to detect INF195 and compound **5**. As could be expected on the basis of their molecular properties (INF195 ClogP = 3,34; compound **5** ClogP = 2,35, $ClogD^{7.4} = -0.61$), compound **5** was not detected inside the cell while INF195 was indeed able to permeate the cell membrane and was largely hydrolyzed to its active metabolite in the cytosol. The amount of parent INF195 and its active metabolite **5**, expressed as ng/mg proteins, is reported in Table 2. After 2 h, the molar ratio **5**/INF195 is approximately 6.6, this indicate that the hydrolysis of INF195 to its active metabolite **5** inside H9c2 takes place in a time comparable to that used in the IRI experiments. Notably, none of the compounds was detected in the mitochondrial fraction.

On the basis of these results, we selected compound INF195 for further studies.

3.7. Low doses of INF195 protect mice hearts after myocardial IRI in ex vivo heart model

Compound INF195, the ethyl ester prodrug of **5**, was selected for *ex vivo* experiments owing to its cell permeability.

First, the cytotoxicity exerted by INF195 was evaluated using the MTT assay in H9c2 cells at increasing concentrations (INF195 0.1–1–5-10-20-50 μM) for 24 h. No effects on cardiomyoblast viability were observed even for the highest concentration of INF195 tested (data not shown). The stability of INF195 in the perfusion fluid (KHB) was then

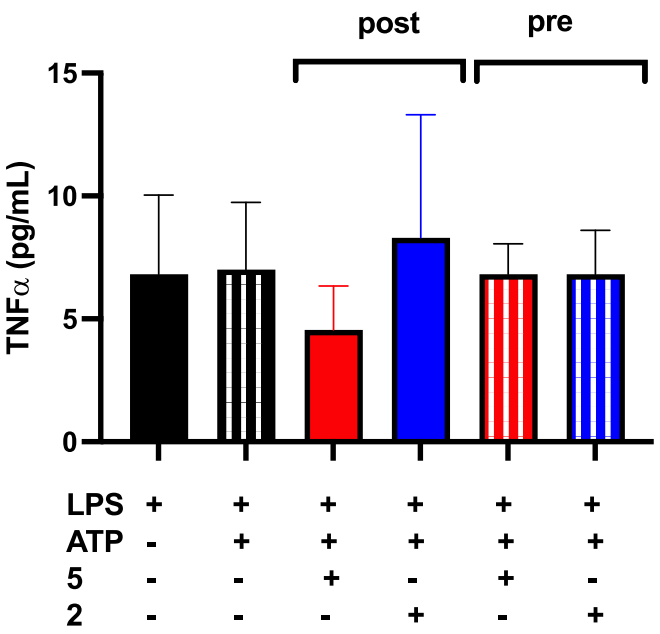

Fig. 6. - Effect of compounds **2** (INF195) and **5** (10 μM) on TNF-α release from differentiated THP-1 stimulated with LPS/ATP. Post: compounds are incubated for 1 h after LPS treatment; pre: compounds are incubated for 10 min before LPS treatment. Data are the mean ± SEM of three independent experiments.

Table 2
Cellular permeation of INF195 (**2**) and **5** in H9c2 cardiomyoblasts. [a] Compounds were incubated at 10 μM concentration in fresh medium for 2 h. [b] Compounds were detected by UHPLC/MS/MS in cytosolic and mitochondrial fractions.

Compound	Conc (μM) [a]	Cytosolic fraction[b] (ng/mg prot)	Mitochondrial fraction[b] (ng/mg prot)
5	10	Not detected	Not detected
INF195 (**2**)	10	**5**: 17.4 INF195 (**2**): 2.88	Not detected

checked by incubating INF195 for 24 h in the perfusion buffer. The amount of remaining compound was detected by UHPLC/MS/MS. In this condition, INF195 was completely stable for 2 h. The hydrolyzed compound **5** was detected in traces (<1%) after 4 h while a 10% of this metabolite was measured after 24 h of incubation (Fig. S4). These results indicated that INF195 is stable in the perfusion fluid for the time employed in IRI experiments.

To explore the potential protective effect against myocardial injury, we evaluated the decrease in infarct size (IS) after pre-treatment with

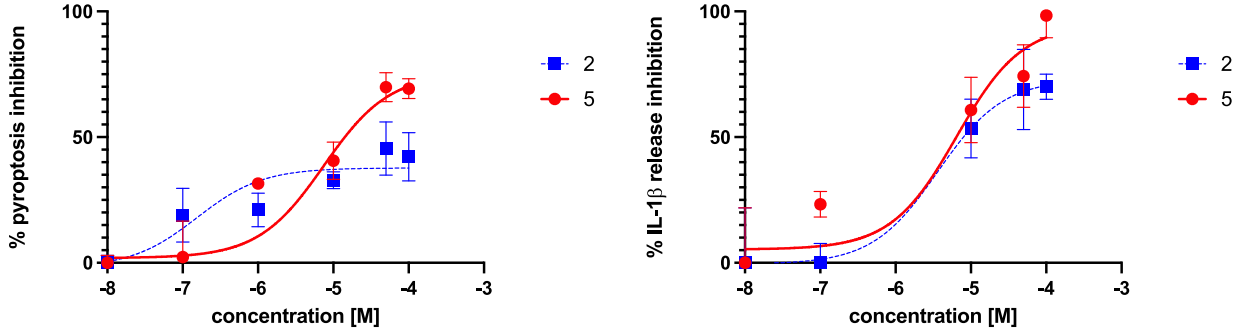

Fig. 5. Concentration-response curves for compounds **2** (INF195) and **5**. (A) prevention of pyroptotic cell death evoked by increasing concentration (0.01–100 μM) of tested compounds; (B) inhibition of IL-1β release evoked by increasing concentration (0.01–100 μM) of tested compounds. Data are the mean ± SEM of three independent experiments.

different concentration of INF195.

The IS of the IR group was 64,8 ± 1,9% of the risk area, the infusion of INF195 at 5 μM reduced significantly IS to 38.1 ± 1.3% of the risk area ($p < 0,0001$ *vs* IR). Also, the infusion of INF195 at 10 μM reduced IS significantly to 48.5 ± 2.9% of the risk area ($p < 0,001$ *vs* IR; p = n.s. *vs* INF195–5 μM) (Fig. 7). However, INF195 at 20 μM did not reduce IS, which resulted similar to the IR group being 66.6 ± 3.5 of the risk area.

In line with previous studies showing the efficacy of NLRP3 inhibitors in the cardiovascular field [10,20–23,38–40], we observed a significant reduction in infarct size using the 5 and 10 μM concentrations of INF195. Of note, the higher used dose did not produce any protective effect: in this case, the amount of necrotic tissue was comparable to that of hearts from the untreated group. The *ex vivo* enabled us to study the inhibitor's intra-organ effects, excluding any blood cell interference. Indeed, the isolated heart is considered an appropriate model for assessing treatment efficacy in reducing myocardial IRI [28,41].

Data are mean ± SEM. *** $p < 0.001$ *vs* IR; **** $p < 0.0001$ *vs* IR; $^{\$\$\$\$}$ $p < 0.0001$ *vs* INF195 5 μM; $^{\#\#\#}$ $p < 0.001$ *vs* INF195 10 μM.

3.8. Pre-treatment with INF195 Reduces Downstream Signaling of the NLRP3 Inflammasome

Triggering signals in cardiovascular disorders result in NLRP3 inflammasome assembly, caspase-1 activation and cleavage of pro-IL-1β into mature IL-1β [6,7,15,42]. Therefore, we investigated the levels of active caspase-1 and IL-1β in the hearts treated or not with the developed inhibitor INF195. The data relative to the release of IL-1β and cleaved caspase-1 (indices of NLRP3 activation) are reported in Fig. 8. The analysis of post-ischemic myocardial tissue revealed that isolated hearts treated with INF195 at 5 and 10 μM showed a significant reduction in IL-1β levels compared with the IR group ($p < 0.05$ *vs* IR for both) (Fig. 8A). Of note, at the highest tested dose (20 μM), the reduction in IL-1β expression levels did not reach statistical significance. The reduction of cleaved caspase-1 observed in the INF195-treated groups was not significant with respect to IR (Fig. 8B), although a clear trend toward reduction can be seen in all the treatment groups. Given that decreased IL-1β release and caspase-1 cleavage indicate diminished pyroptosis [7,15,31], it follows that effective doses might reduce infarct size by stopping cell death through pyroptosis.

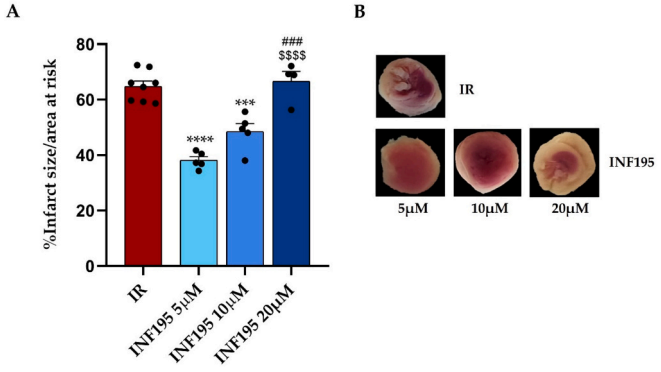

Fig. 7. Infarct size in hearts from mice exposed to 30 min of ischemia followed by 60 min of reperfusion, pretreated (INF195) or not (IR) with 5, 10 or 20 μM INF195 in the perfusate 10 min before ischemia. **A)** Infarct size after IR exposition is expressed as a percentage of area at risk of mice hearts. Black circles depict individual hearts, whereas colored bars show group means and SEM. **B)** Representative pictures of left ventricle slices of mice of the different experimental groups. The area at risk is indicated in red, while the infarct area in white. (For interpretation of the references to colour in this figure legend, the reader is referred to the web version of this article.)

3.9. Correlation between levels of IL-1β and cleaved caspase-1 in infarcted heart tissues and Infarct Size

Surprisingly, we only found a significant correlation between IL-1β and infarct size (Fig. 9A; $p = 0.0298$). Caspase-1 did not show a strong correlation with infarct size (Fig. 9B). The lack of a significant correlation between levels of cleaved caspase-1 and infarct size, despite the expected association between caspase-1 activation and pyroptosis-mediated cell death, suggests the influence of various potential factors. This absence of correlation could stem from differences in spatial distribution, temporal dynamics, and/or regulatory mechanisms governing caspase-1 activation and its role in myocardial infarction progression. Future studies could clarify this issue.

According to the literature, the triggering of pro-inflammatory caspase-1 induces the maturation of IL-1β [43]. This latter evidence is confirmed in our study, which reveals a large amount of IL-1β in IR hearts group. The level of this cytokine is significantly reduced in hearts treated with 5 or 10 μM of INF195. On the contrary, the 20 μM concentration does not induce a significant decrease with respect to the IR group. Notably, based on our hypothesis, in INF195-treated hearts, the levels of cleaved caspase-1 remain approximately 50% lower than IR group, although not reaching statistical significance. Nevertheless, the trend in reduction of these factors is inversely related to the dose used (Fig. 9), suggesting a dual role of the inhibitor. We cannot rule out the influence of INF195 in other pathways at the maximum employed dose. Indeed, several pathways can lead to caspase-1 and IL-1β expression, including the activation of the STAT signaling pathway [44], which is a pathway with multiple protective and/or damaging facets in the IR scenario [45]. In future studies, it will be necessary to ascertain whether INF195 interferes with STAT signaling and whether it does so in a protective or deleterious way. The current study focused primarily on the efficacy of INF195 in reducing NLRP3-dependent pyroptosis and IL-1β release *in vitro* and its effects on myocardial infarct size in murine hearts. However, extrapolating these findings to clinical settings requires further investigation into the drug's pharmacokinetic properties and long-term safety profile in human subjects.

4. Conclusion

The activation of the NLRP3 inflammasome has been strongly linked to various cardiovascular diseases [7,46,47]. In acute scenarios, inhibiting NLRP3 inflammasome activity holds promise for preserving viable cardiac tissue, offering significant therapeutic benefits [47]. In our study, we utilized advanced computational techniques to design a novel series of NLRP3 inhibitors, leading to the discovery of INF195, a non-covalent inhibitor. INF195 has shown remarkable efficacy in reducing NLRP3-dependent pyroptosis and IL-1β release in human macrophages. We demonstrated that even low doses of INF195 reduces IL-1β formation *ex vivo* after ischemia-reperfusion, reflecting in reduced infarct size area in isolated murine hearts. However, a dual effect of INF195 has emerged at higher dose, resulting in a loss of cardioprotective efficacy. Notably, the structural diversity of INF195 compared to sulfonylurea-based inhibitors [48] opens the possibility for further modulation of this pharmacophore to optimize and improve its activity. Indeed, targeting the NLRP3 inflammasome with INF195 emerges as a promising strategy for tissue preservation in the myocardial IRI scenario. Importantly, the administration of low doses of INF195 significantly reduces IL-1β formation post-reperfusion, correlating with diminished myocardial infarct size and suggesting a potential mitigation of inflammatory processes. While having a drug that is effective at low doses is advantageous, the observed dual effect of INF195 at higher doses underscores the need for thorough investigation to fully understand its implications. Specifically, further studies are needed to fully clarify whether the reduced effectiveness at higher doses of INF195 is due to off-target effects, which may counteract its protective action, or stems from the dual role (deleterious and protective) of NLRP3. Future investigations exploring the effects of

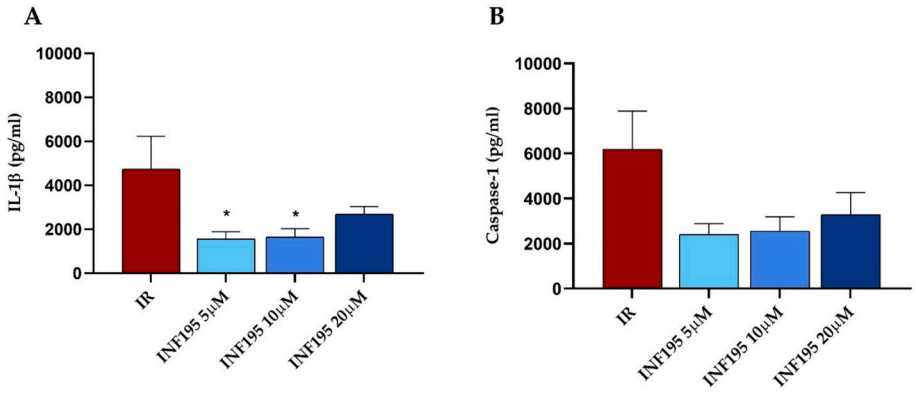

Fig. 8. IL-1β (A) and caspase-1 (B) concentrations evaluated by ELISA in extracts of left ventricular apex from mice exposed to IR pretreated or not with INF195. Data are presented as the means ± SEM. Statistical significance: *p < 0.05 *vs* IR.

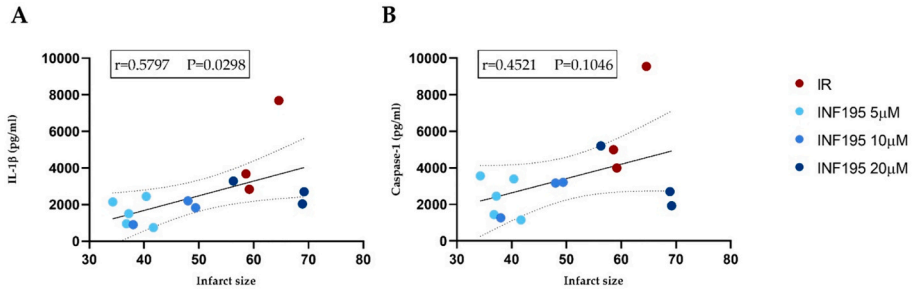

Fig. 9. Correlation graphs between **A)** cardiac IL-1β and infarct size and **B)** cardiac caspase-1 and infarct size in mice exposed to IR, pretreated or not with INF195.

the NLRP3 inhibitor on a broader spectrum of cytokines and inflammatory mediators beyond IL-1β could provide valuable insights into its mechanism of action and potential therapeutic applications.

Ethics approval and consent to participate

The animals were maintained following the European Directive 2010/63/EU about the protection of animals being used for research reasons.

Consent for publication

All the authors read and approved the final version of the manuscript.

Funding

The authors thank grant H2020-SGA-FETFLAG-HBP-2019-BRAVE project - FPA No: 650003, Specific Agreement number: 945539, HBP SGA3, for providing support for this research.

FS thanks the Centre for HPC, Big Data and Quantum Computing, finanziato dal Decreto Direttoriale di concessione del finanziamento n.1031 del 17.06.2022." This work was supported from University of Turin, Ricerca Locale 2021, 2022 (BERM_RILO_21_01; SPY_RILO_21_01; SPY_RILO_22_01; MARE_RILO_22_01), and Grant for Internationalization – GFI (MARE_GFI_22_01_F; MARE_GFI_22_01_F_01). Progetti PRIN: PAGP_PRIN_2022_23_01 - 2022AA37N3. BERM_PRIN_2022_23_02 - 20229WP2JJ. PENC_PRIN_2022_23_01-2022S74XWB.

CRediT authorship contribution statement

Simone Gastaldi: Investigation. **Magalì Giordano:** Investigation. **Federica Blua:** Investigation. **Chiara Rubeo:** Investigation. **Valentina Boscaro:** Investigation. **Saveria Femminò:** Investigation, Writing – review & editing. **Stefano Comità:** Investigation. **Eleonora Gianquinto:** Visualization, Methodology, Investigation. **Vanessa Landolfi:** Investigation. **Elisabetta Marini:** Investigation, Funding acquisition. **Margherita Gallicchio:** Validation, Methodology. **Francesca Spyrakis:** Supervision, Funding acquisition. **Pasquale Pagliaro:** Writing – review & editing, Supervision, Funding acquisition, Conceptualization. **Massimo Bertinaria:** Writing – review & editing, Writing – original draft, Supervision, Funding acquisition, Conceptualization. **Claudia Penna:** Writing – original draft, Supervision, Funding acquisition, Conceptualization.

Declaration of competing interest

The authors declare that they have no known competing financial interests or personal relationships that could have appeared to influence the work reported in this paper.

Data availability

The datasets generated and analyzed for this study are available from the corresponding author upon reasonable request.

Acknowledgments

We acknowledge the use of Fenix Infrastructure resources, which are partially funded from the European Union's Horizon 2020 research and innovation programme through the ICEI project under the grant agreement No. 800858 (Application No. 25681). We kindly thank BiKi technologies for providing the BiKi Life Science suite. Simone Gastaldi and Eleonora Gianquinto acknowledge Horizon 2020 Framework Programme, Specific Grant Agreement No. 945539 (Human Brain Project SGA3) for the post-doc positions. We thank prof. Loretta Lazzarato and

prof. Barbara Rolando for assistance with the HPLC/MS analysis.

Appendix A. Supplementary data

Supplementary data to this article can be found online at https://doi.org/10.1016/j.vph.2024.107397.

References

[1] C.J. Zuurbier, A. Abbate, H.A. Cabrera-Fuentes, M.V. Cohen, M. Collino, D.P.V. De Kleijn, et al., Innate immunity as a target for acute cardioprotection, Cardiovasc. Res. 115 (2019) 1131–1142, https://doi.org/10.1093/cvr/cvy304.

[2] P. Pagliaro, F. Moro, F. Tullio, M.G. Perrelli, C. Penna, Cardioprotective pathways during reperfusion: focus on redox signaling and other modalities of cell signaling, Antioxid. Redox Signal. 14 (2011) 833–850, https://doi.org/10.1089/ars.2010.3245.

[3] G. Heusch, Myocardial ischaemia-reperfusion injury and cardioprotection in perspective, Nat. Rev. Cardiol. 17 (2020) 773–789, https://doi.org/10.1038/s41569-020-0403-y.

[4] A.J. Ludman, D.M. Yellon, D.J. Hausenloy, Cardiac preconditioning for ischaemia: lost in translation, Dis. Model. Mech. 3 (2010) 35–38, https://doi.org/10.1242/dmm.003855.

[5] F. Tullio, C. Angotti, M.G. Perrelli, C. Penna, P. Pagliaro, Redox balance and cardioprotection, Basic Res. Cardiol. 108 (2013) 392, https://doi.org/10.1007/s00395-013-0392-7.

[6] E. Mezzaroma, A. Abbate, S. Toldo, NLRP3 inflammasome inhibitors in cardiovascular diseases, Molecules 26 (2021) 976, https://doi.org/10.3390/molecules26040976.

[7] S. Toldo, A. Abbate, The role of the NLRP3 inflammasome and pyroptosis in cardiovascular diseases, Nat. Rev. Cardiol. (2023), https://doi.org/10.1038/s41569-023-00946-3. Nov 3.

[8] C. Gollmann-Tepeköylü, M. Graber, L. Pölzl, F. Nägele, R. Moling, H. Esser, B. Summerer, V. Mellitzer, S. Ebner, J. Hirsch, et al., Toll-like receptor 3 mediates ischaemia/reperfusion injury after cardiac transplantation, Eur. J. Cardiothorac. Surg. 57 (2020) 826–835, https://doi.org/10.1093/ejcts/ezz383.

[9] Ø. Sandanger, T. Ranheim, L.E. Vinge, M. Bliksøen, K. Alfsnes, A.V. Finsen, C. P. Dahl, E.T. Askevold, G. Florholmen, G. Christensen, et al., The NLRP3 inflammasome is up-regulated in cardiac fibroblasts and mediates myocardial ischaemia-reperfusion injury, Cardiovasc. Res. 99 (2013) 164–174, https://doi.org/10.1093/cvr/cvt091.

[10] R. Mastrocola, C. Penna, F. Tullio, S. Femminò, D. Nigro, F. Chiazza, L. Serpe, D. Collotta, G. Alloatti, M. Cocco, et al., Pharmacological inhibition of NLRP3 Inflammasome attenuates myocardial ischemia/reperfusion injury by activation of RISK and mitochondrial pathways, Oxidative Med. Cell. Longev. 2016 (2016) 5271251, https://doi.org/10.1155/2016/5271251.

[11] C. Penna, M. Aragno, A.S. Cento, S. Femminò, I. Russo, F.D. Bello, F. Chiazza, D. Collotta, G.F. Alves, M. Bertinaria, et al., Ticagrelor conditioning effects are not additive to Cardioprotection induced by direct NLRP3 Inflammasome inhibition: role of RISK, NLRP3, and redox cascades, Oxidative Med. Cell. Longev. 2020 (2020) 9219825, https://doi.org/10.1155/2020/9219825.

[12] R. Mastrocola, M. Collino, C. Penna, D. Nigro, F. Chiazza, V. Fracasso, F. Tullio, G. Alloatti, P. Pagliaro, M. Aragno, Maladaptive modulations of NLRP3 Inflammasome and Cardioprotective pathways are involved in diet-induced exacerbation of myocardial ischemia/reperfusion injury in mice, Oxidative Med. Cell. Longev. 2016 (2016) 3480637, https://doi.org/10.1155/2016/3480637.

[13] I.V. Hochheiser, M. Pilsl, G. Hagelueken, J. Moecking, M. Marleaux, R. Brinkschulte, E. Latz, C. Engel, M. Geyer, Structure of the NLRP3 decamer bound to the cytokine release inhibitor CRID3, Nature 604 (2022) 184–189, https://doi.org/10.1038/s41586-022-04467-w.

[14] C. Pellegrini, A. Martelli, L. Antonioli, M. Fornai, C. Blandizzi, V. Calderone, NLRP3 inflammasome in cardiovascular diseases: pathophysiological and pharmacological implications, Med. Res. Rev. 41 (2021) 1890–1926, https://doi.org/10.1002/med.21781.

[15] S. Toldo, A.G. Mauro, Z. Cutter, A. Abbate, Inflammasome, pyroptosis, and cytokines in myocardial ischemia-reperfusion injury, Am. J. Physiol. Heart Circ. Physiol. 315 (2018) H1553–H1568, https://doi.org/10.1152/ajpheart.00158.2018.

[16] Y-J. Bai, Z-G. Li, W.H. Liu, D. Gao, P.Y. Zhang, M. Liu. Effects of IL-1β and IL-18 induced by NLRP3 inflammasome activation on myocardial reperfusion injury after PCI. Eur. Rev. Med. Pharmacol. Sci. 23 (2019) 10101–10106. doi: 10.26355/eurrev_201911_19579.

[17] Y. Tong, Z. Wang, L. Cai, L. Lin, J. Liu, J. Cheng, NLRP3 Inflammasome and its central role in the cardiovascular diseases, Oxidative Med. Cell. Longev. 2020 (2020) 4293206, https://doi.org/10.1155/2020/4293206.

[18] C.J. Zuurbier, NLRP3 Inflammasome in Cardioprotective signaling, J. Cardiovasc. Pharmacol. 74 (2019) 271–275, https://doi.org/10.1097/FJC.0000000000000696.

[19] P. Pagliaro, C. Penna, Inhibitors of NLRP3 Inflammasome in ischemic heart disease: focus on functional and redox aspects, Antioxidants (Basel). 12 (2023) 1396, https://doi.org/10.3390/antiox12071396.

[20] S. Toldo, A.G. Mauro, Z. Cutter, B.W. Van Tassell, E. Mezzaroma, M.G. Del Buono, A. Prestamburgo, N. Potere, A. Abbate, The NLRP3 Inflammasome inhibitor, OLT1177 (Dapansutrile), reduces infarct size and preserves contractile function after ischemia reperfusion injury in the mouse, J. Cardiovasc. Pharmacol. 73 (2019) 215–222, https://doi.org/10.1097/FJC.0000000000000658.

[21] S. Toldo, C. Marchetti, A.G. Mauro, J. Chojnacki, E. Mezzaroma, S. Carbone, S. Zhang, B. Van Tassell, F.N. Salloum, A. Abbate, Inhibition of the NLRP3 inflammasome limits the inflammatory injury following myocardial ischemia-reperfusion in the mouse, Int. J. Cardiol. 209 (2016) 215–220, https://doi.org/10.1016/j.ijcard.2016.02.043.

[22] C. Marchetti, J. Chojnacki, S. Toldo, E. Mezzaroma, N. Tranchida, S.W. Rose, M. Federici, B.W. Van Tassell, S. Zhang, A. Abbate, A novel pharmacologic inhibitor of the NLRP3 inflammasome limits myocardial injury after ischemia-reperfusion in the mouse, J. Cardiovasc. Pharmacol. 63 (2014) 316–322, https://doi.org/10.1097/FJC.0000000000000053.

[23] C. Penna, S. Femminò, F. Caldera, A. Rubin Pedrazzo, C. Cecone, E. Alfì, S. Comità, T. Higashiyama, F. Trotta, P. Pagliaro, et al., Cyclic Nigerosyl-Nigerose as oxygen Nanocarrier to protect cellular models from hypoxia/Reoxygenation injury: implications from an in vitro model, Int. J. Mol. Sci. 22 (2021) 4208, https://doi.org/10.3390/ijms22084208.

[24] S. Gargiulo, A. Greco, M. Gramanzini, S. Esposito, A. Affuso, A. Brunetti, G. Vesce, Mice anesthesia, analgesia, and care, part I: anesthetic considerations in preclinical research, ILAR J. 53 (1) (2012) E55–E69, https://doi.org/10.1093/ilar.53.1.55.

[25] C. Penna, M. Sorge, F. Tullio, S. Comità, S. Femminò, M. Brancaccio, P. Pagliaro, A TRICk to improve the effectiveness of RIC: role of limb temperature in enhancing the effectiveness of remote ischemic conditioning, Biology (Basel). 11 (2022) 146, https://doi.org/10.3390/biology11010146.

[26] C. Penna, M. Brancaccio, F. Tullio, C. Rubinetto, M.G. Perrelli, C. Angotti, P. Pagliaro, G. Tarone, Overexpression of the muscle-specific protein, melusin, protects from cardiac ischemia/reperfusion injury, Basic Res. Cardiol. 109 (2014) 418, https://doi.org/10.1007/s00395-014-0418-9.

[27] A.A. Bulhak, C. Jung, C.G. Ostenson, J.O. Lundberg, P.O. Sjöquist, J. Pernow, PPAR-alpha activation protects the type 2 diabetic myocardium against ischemia-reperfusion injury: involvement of the PI3-kinase/Akt and NO pathway, Am. J. Physiol. Heart Circ. Physiol. 296 (2009) H719–H727, https://doi.org/10.1152/ajpheart.00394.2008.

[28] H.E. Bøtker, D. Hausenloy, I. Andreadou, S. Antonucci, K. Boengler, S.M. Davidson, S. Deshwal, Y. Devaux, F. Di Lisa, M. Di Sante, et al., Practical guidelines for rigor and reproducibility in preclinical and clinical studies on cardioprotection, Basic Res. Cardiol. 113 (2018) 39, https://doi.org/10.1007/s00395-018-0696-8.

[29] F. D'Ascenzo, S. Femminò, F. Ravera, F. Angelini, A. Caccioppo, L. Franchin, A. Grosso, S. Comità, C. Cavallari, C. Penna, et al., Extracellular vesicles from patients with acute coronary syndrome impact on ischemia-reperfusion injury, Pharmacol. Res. 170 (2021) 105715, https://doi.org/10.1016/j.phrs.2021.105715.

[30] M.F. Balaha, N.J. Ahmed, Z.S. Almalki, A.K. Alahmari, A.M. Alshehri, G. A. Soliman, A.M. Hamad, Epimedin a ameliorates DNFB-induced allergic contact dermatitis in mice: role of NF-κB/NLRP3-driven pyroptosis, Nrf2/HO-1 pathway, and inflammation modulation, Life Sci. 302 (2022) 120653, https://doi.org/10.1016/j.lfs.2022.120653.

[31] M. Cocco, D. Garella, A. Di Stilo, E. Borretto, L. Stevanato, M. Giorgis, E. Marini, R. Fantozzi, G. Miglio, M. Bertinaria, Electrophilic warhead-based design of compounds preventing NLRP3 inflammasome-dependent pyroptosis, J. Med. Chem. 57 (2014) 10366–10382, https://doi.org/10.1021/jm501072b.

[32] M. Cocco, C. Pellegrini, H. Martínez-Banaclocha, M. Giorgis, E. Marini, A. Costale, G. Miglio, M. Fornai, L. Antonioli, G. López-Castejón, et al., Development of an acrylate derivative targeting the NLRP3 Inflammasome for the treatment of inflammatory bowel disease, J. Med. Chem. 60 (2017) 3656–3671, https://doi.org/10.1021/acs.jmedchem.6b01624.

[33] C. Pellegrini, M. Fornai, R. Colucci, L. Benvenuti, V. D'Antongiovanni, G. Natale, F. Fulceri, M. Giorgis, E. Marini, S. Gastaldi, et al., A comparative study on the efficacy of NLRP3 Inflammasome signaling inhibitors in a pre-clinical model of bowel inflammation, Front. Pharmacol. 9 (2018) 1405, https://doi.org/10.3389/fphar.2018.01405.

[34] S. Gastaldi, V. Boscaro, E. Gianquinto, C.F. Sandall, M. Giorgis, E. Marini, F. Blua, M. Gallicchio, F. Spyrakis, J.A. MacDonald, et al., Chemical modulation of the 1-(Piperidin-4-yl)-1,3-dihydro-2*H*-benzo[d]imidazole-2-one scaffold as a novel NLRP3 inhibitor, Molecules 26 (2021) 3975, https://doi.org/10.3390/molecules26133975.

[35] S. Gastaldi, C. Rocca, E. Gianquinto, M.C. Granieri, V. Boscaro, F. Blua, B. Rolando, E. Marini, M. Gallicchio, A. De Bartolo, et al., Discovery of a novel 1,3,4-oxadiazol-2-one-based NLRP3 inhibitor as a pharmacological agent to mitigate cardiac and metabolic complications in an experimental model of diet-induced metaflammation, Eur. J. Med. Chem. 257 (2023) 115542, https://doi.org/10.1016/j.ejmech.2023.115542.

[36] C. Dekker, H. Mattes, M. Wright, A. Boettcher, A. Hinniger, N. Hughes, S. Kapps-Fouthier, J. Eder, P. Erbel, N. Stiefl, et al., Crystal structure of NLRP3 NACHT domain with an inhibitor defines mechanism of Inflammasome inhibition, J. Mol. Biol. 433 (2021) 167309, https://doi.org/10.1016/j.jmb.2021.167309.

[37] D. Harrison, N. Boutard, K. Brzozka, M. Bugaj, S. Chmielewski, A. Cierpich, J. R. Doedens, C.R.Y. Fabritius, C.A. Gabel, M. Galezowski, et al., Discovery of a series of ester-substituted NLRP3 inflammasome inhibitors, Bioorg. Med. Chem. Lett. 30 (2020) 127560, https://doi.org/10.1016/j.bmcl.2020.127560.

[38] Y. Liu, K. Lian, L. Zhang, R. Wang, F. Yi, C. Gao, C. Xin, D. Zhu, Y. Li, W. Yan, et al., TXNIP mediates NLRP3 inflammasome activation in cardiac microvascular endothelial cells as a novel mechanism in myocardial ischemia/reperfusion injury, Basic Res. Cardiol. 109 (2014) 415, https://doi.org/10.1007/s00395-014-0415-z.

[39] J. Aliaga, A. Bonaventura, E. Mezzaroma, Y. Dhakal, A.G. Mauro, A. Abbate, S. Toldo, Preservation of contractile reserve and diastolic function by inhibiting the

NLRP3 Inflammasome with OLT1177® (Dapansutrile) in a mouse model of severe ischemic cardiomyopathy due to non-Reperfused Anterior Wall myocardial infarction, Molecules 26 (2021) 3534, https://doi.org/10.3390/molecules26123534.

[40] S. Toldo, C. Marchetti, A.G. Mauro, J. Chojnacki, E. Mezzaroma, S. Carbone, S. Zhang, B. Van Tassell, F.N. Salloum, A. Abbate, Inhibition of the NLRP3 inflammasome limits the inflammatory injury following myocardial ischemia-reperfusion in the mouse, Int. J. Cardiol. 209 (2016) 215–220, https://doi.org/10.1016/j.ijcard.2016.02.043.

[41] R.M. Bell, M.M. Mocanu, D.M. Yellon, Retrograde heart perfusion: the Langendorff technique of isolated heart perfusion, J. Mol. Cell. Cardiol. 50 (2011) 940–950, https://doi.org/10.1016/j.yjmcc.2011.02.018.

[42] S. Merkle, S. Frantz, M.P. Schön, J. Bauersachs, M. Buitrago, R.J. Frost, E. M. Schmitteckert, M.J. Lohse, S. Engelhardt, A role for caspase-1 in heart failure, Circ. Res. 100 (2007) 645–653, https://doi.org/10.1161/01.RES.0000260203.55077.61.

[43] P. Broz, V.M. Dixit, Inflammasomes: mechanism of assembly, regulation and signalling, Nat. Rev. Immunol. 16 (2016) 407–420, https://doi.org/10.1038/nri.2016.58.

[44] Y.E. Chin, M. Kitagawa, K. Kuida, R.A. Flavell, X.Y. Fu, Activation of the STAT signaling pathway can cause expression of caspase 1 and apoptosis, Mol. Cell. Biol. 17 (1997) 5328–5337, https://doi.org/10.1128/MCB.17.9.5328.

[45] S. Comità, S. Femmino, C. Thairi, G. Alloatti, K. Boengler, P. Pagliaro, C. Penna, Regulation of STAT3 and its role in cardioprotection by conditioning: focus on non-genomic roles targeting mitochondrial function, Basic Res. Cardiol. 116 (2021) 56, https://doi.org/10.1007/s00395-021-00898-0.

[46] A. Abbate, S. Toldo, C. Marchetti, J. Kron, B.W. Van Tassell, C.A. Dinarello, Interleukin-1 and the Inflammasome as therapeutic targets in cardiovascular disease, Circ. Res. 126 (2020) 1260–1280, https://doi.org/10.1161/CIRCRESAHA.120.315937.

[47] A. Sharma, M. Tate, G. Mathew, J.E. Vince, R.H. Ritchie, J.B. de Haan, Oxidative stress and NLRP3-Inflammasome activity as significant drivers of diabetic cardiovascular complications: therapeutic implications, Front. Physiol. 9 (2018) 114, https://doi.org/10.3389/fphys.2018.00114.

[48] N. Li, R. Zhang, M. Tang, M. Zhao, X. Jiang, X. Cai, N. Ye, K. Su, J. Peng, X. Zhang, W. Wu, H. Ye, Recent Progress and prospects of small molecules for NLRP3 Inflammasome inhibition, J. Med. Chem. 66 (2023) 14447–14473, https://doi.org/10.1021/acs.jmedchem.3c01370.